Valentin Ludwig[1] and Thomas Krumpen[1]

[1]Alfred Wegener Institute, Helmholtz Centre for Polar and Marine Research

January 11, 2025

Highlights

Coverage Varies, Origin Shifts: 37 Years of Sea-Ice Conditions at the HAUSGARTEN Observatory

Valentin Ludwig, Thomas Krumpen

- Sea ice coverage over HAUSGARTEN moorings fluctuates but shows no significant long-term trend
- Sea-ice age over HAUSGARTEN moorings declines
- Sea-ice origin of ice passing HAUSGARTEN has shifted northward over time

Coverage Varies, Origin Shifts: 37 Years of Sea-Ice Conditions at the HAUSGARTEN Observatory

Valentin Ludwig[a], Thomas Krumpen[a]

[a] *Alfred Wegener Institute, Helmholtz Centre for Polar and Marine Research, Am Handelshafen 12, Bremerhaven, 27570, Bremen, Germany*

Abstract

The HAUSGARTEN observatory consists of 21 moorings equipped with a wide range of sensors that, since 1999, have been monitoring abiotic and biotic processes in Fram Strait. As the Transpolar Drift continuously conveys sea ice from the central Arctic Ocean toward Fram Strait, some mooring sites are covered seasonally or even year-round by closed ice pack. Previous studies have shown that when sea ice is present, it can exert direct or indirect effects on the underlying water column, extending all the way down to the seafloor. In this manuscript, we provide an overview and a more thorough assessment of the sea-ice conditions at the N3–5 and EGI-IV moorings, focusing on both seasonal variability and long-term changes. The EGI-IV moorings are located farther west and show significantly higher ice coverage, whereas the N3-5 moorings located farther to the northeast persistently exhibit lower ice concentrations. Somewhat unexpectedly, and in contrast to the rest of the Arctic, sea-ice concentration at these mooring sites shows no significant trends—neither on an annual nor on a monthly timescale. This is because the presence of sea ice above the moorings is primarily governed by geostrophic winds that drive ice export between Greenland and Spitsbergen. Although no direct changes in ice coverage are apparent, noticeable changes in ice properties do occur. On the one hand, the age of the ice at both locations has declined sharply; on the other hand, its origin has shifted northward, thereby reducing the proportion of ice formed in shallow-water regions and interrupting the transport of ice-rafted matter from the Siberian shelves towards Fram Strait.

Email address: valentin.ludwig@awi.de (Valentin Ludwig)

Preprint submitted to Deep Sea Research Part II: Topical Studies in Oceanography2024-12-27

Keywords: sea-ice concentration, sea-ice origin, sea-ice age, trend analysis, HAUSGARTEN

1. Introduction

The HAUSGARTEN observatory is an array of 21 moorings located in the eastern Fram Strait, at approximately 79°N and 5°W to 10°E (see Fig. 1). The moorings are deployed at depths between 1000 m and 5600 m and are equipped with a wide range of sensors to monitor hydrographic conditions as well as abiotic and biotic vertical fluxes (e.g., carbonate, particulate organic carbon and nitrogen, biogenic silica, biomarkers). HAUSGARTEN has been operated by the Alfred Wegener Institute since 1999 (Soltwedel et al., 2005), providing valuable long-term time series of ecological processes in this highly dynamic region (Swoboda et al., 2024). The mooring arrays are located in a confluence zone where warm, saline Atlantic water flows northward to meet cold, low-salinity Arctic water masses. Some of the moorings remain permanently or seasonally covered by sea ice that exits the Arctic through this gateway and eventually melts.

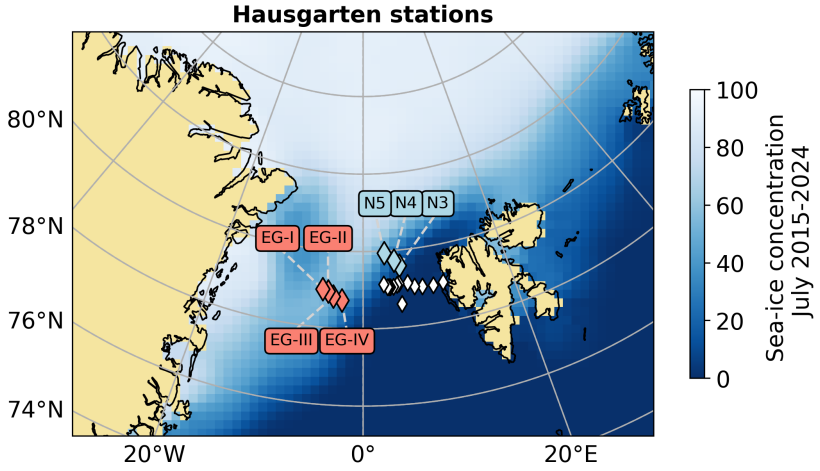

Figure 1: Overview of the HAUSGARTEN stations, indicated by diamonds. Our analysis is limited to the EG moorings (red labels) and the N moorings (blue labels). The other moorings are shown as smaller white diamonds. The background shows the mean July sea-ice concentration from the OSI SAF 450-a/430-a product between 2015 and 2024.

Estimates suggest that about 10 % of the Arctic's sea ice is exported annually via Fram Strait (Smedsrud et al., 2017), making this region particularly

important for long-term monitoring programs aimed at assessing the impacts of global warming on sea ice in the central Arctic Ocean (Sumata et al., 2023; Krumpen et al., 2025). The export of sea ice through Fram Strait is driven by strong geostrophic winds, which result from the sea-level pressure gradient between Spitsbergen and Greenland and lead to southward-directed ice drift. As a result of the continuous export of sea ice, the N3-5 and EGI-IV moorings in particular are frequently covered by ice. Sea ice in Fram Strait originates from multiple regions of the Arctic and can thus display high temporal and spatial variability in its properties (Belter et al., 2021). In the eastern Fram Strait where N3-5 and EGI-IV are located, however, most of the ice originates from the Russian shelf seas and is conveyed via the Transpolar Drift to the HAUSGARTEN observatory. Many studies have addressed how this steady outflow of sea ice from the Arctic has changed over time. Following Smedsrud et al. (2017), for instance, the amount of ice exported through Fram Strait has increased by about 6 % per decade, driven by stronger southward ice drift speeds due to enhanced geostrophic winds (largely explained by increasing surface pressure over Greenland). In particular spring and summer show larger changes in ice export compared to autumn and winter. Other satellite- or model-based studies covering longer time periods report comparable (Zamani et al., 2019; Smedsrud et al., 2011), stronger (Krumpen et al., 2016), or no significant changes (Kwok et al., 2013).

The influence of sea ice on the composition and variability of organic and inorganic fluxes observed at the HAUSGARTEN observatory has been investigated in various studies. Recent work has focused on the relationship between locally observed litter and microplastics, and sea ice as a potential source. This topic is highly relevant because some of the highest microplastic concentrations in marine environments have been reported in Fram Strait (Bergmann et al., 2017; Botterell et al., 2022). Existing research shows that sea ice can act as an important transport vehicle for litter, which is released during melting periods (Tekman et al., 2017; Roscher et al., 2025). In particular, microplastics trapped in melting sea ice and algae can form fast-sinking aggregates (Bergmann et al., 2023). The impact of changing environmental conditions, especially varying sea-ice conditions in Fram Strait, on microbial composition of sinking particles and benthic communities has been explored by Cardozo-Mino et al. (2023) and Taylor et al. (2016, 2017). Furthermore, Swoboda et al. (2024) investigated the effect of pan-Arctic sea-ice decline on carbon export processes at multiple HAUSGARTEN sites, showing that terrigenous fluxes from melting sea ice in Fram Strait decreased by more

than 80 % over a 13-year record—primarily due to the reduced fraction of sea ice originating in shallow-shelf areas (Krumpen et al., 2019). The role of melting sea ice in shaping the stratification of the water column, and thus the biological carbon pump, is described by von Appen et al. (2021).

Most of these studies have directly compared mooring observations at various depths with overlying ice conditions (e.g., concentration, origin, thickness). However, this approach often neglects the fact that slowly sinking particles can originate far from the study area. To address this limitation, Wekerle et al. (2018) developed a more complex approach for linking sea-ice conditions with mooring data. Using an eddy-resolving ocean–sea-ice model, the authors first determined a "catchment area" at the water surface—whose size depends on the sinking speed and dimensions of the particles—and then assessed the ice conditions within this area.

To better understand the implications of a warming Arctic and rapidly changing sea ice for HAUSGARTEN observations, a more detailed understanding of local ice conditions is important. Despite the abundance of studies on HAUSGARTEN data, a thorough analysis of how sea-ice conditions over the moorings have evolved throughout its 25-year lifetime is lacking. Closing this gap is the primary motivation for our paper. To this end, we extend the time series back to 1987—the advent of daily passive microwave measurements that enable reliable retrieval and retracking of sea-ice conditions. By providing a comprehensive assessment of local sea-ice variability and trends, we aim to lay the groundwork for interpreting mooring observations in future studies.

In our paper, we briefly present the data and methods used in Section 2. Section 3 then provides a thorough analysis of sea-ice concentration variations over individual moorings as well as their larger surroundings. In Section 4, we present time series on the origin and age of the ice arriving at HAUSGARTEN.

In doing so, we address the following research questions:

1. How does the sea-ice concentration over the HAUSGARTEN moorings change between 1987 and 2024?
2. How do sea-ice properties (origin and age) of sea ice drifting over the HAUSGARTEN moorings change during this period?

which we answer in Section 6.

2. Data & Methods

2.1. Moorings

HAUSGARTEN comprises 21 moorings, but only few of them (N3-N5; EG-I to EG-IV) are at least partly covered by sea ice (Fig. 1). We thus limit our analyses to these seven moorings. When collectively referring to the N3-N5 and EG-I to EG-IV moorings, we call them the N and the EG cluster, respectively.

2.2. Sea-ice concentration

We use the sea-ice concentration data provided by the European Organisation for the Exploitation of Meteorological Satellites (EUMETSAT) Ocean and Sea Ice Application Facility (OSI-SAF) at `https://osi-saf.eumetsat.int/products/sea-ice-products` (last access 2024-12 -27). They are based on a combination of passive microwave measurements by the SMMR (Scanning Multi-channel Microwave Radiometer), SSM/I (Special Sensor Microwave/Imager) and SSMIS (Special Sensor Microwave Imager/Sounder) instruments (Lavergne et al., 2022) and provided in the Equal Area Scalable Earth 2 projection (EASE2, Brodzik et al. (2012)) with a grid spacing of 25 km. The OSI SAF 450-a climate data record is used from January 1987 until April 2020, and the OSI SAF 430-a interim climate data record from May 2020 until September 2024. The products are consistent at the transition (Lavergne et al., 2022). For each mooring, we select the closest satellite pixel. The coordinates of both and the distance between them are given in Table 1. The moorings are spaced 16, 21 and 28 km (EG stations) respectively 21 and 35 km (N stations) apart.

2.3. Backtrajectories of sea ice

To determine the age and source area of sea ice passing by the N3-5 and EGI-IV mooring locations, we track sea ice backward in time using a combination of satellite products. This tracking process is facilitated by the Lagrangian drift model IceTrack, previously utilized in Krumpen et al. (2019) under similar experimental setups. Below, we briefly describe the tracking process and the data products applied: Ice was tracked monthly from January 1, 1987, to September 1, 2024 (452 months), originating from two points at the center of the N3-5 and EGI-IV moorings (79°N, 5°W and 79.75°N, 5°E), and tracked for a maximum duration of 7 years. The tracking approach works as follows: sea ice is traced backward on a daily basis until

Station ID	Lon/Lat station	Lon/Lat OSI SAF	Distance [km]
EG-I	-5.371/78.982	-5.301/79.080	11.4
EG-II	-4.647/78.934	-4.044/78.874	14.5
EG-III	-3.915/78.812	-4.044/78.874	7.4
EG-IV	-2.754/78.728	-2.834/78.663	7.4
N5	5.196/79.598	5.528/79.528	10.3
N4	4.468/79.734	4.399/79.771	4.4
N3	3.120/79.944	3.215/80.010	7.6

Table 1: Coordinates for each station (second column), closest satellite pixel (third row) and the distance between them (fourth row).

either (a) the tracked ice reaches the coastline or fast ice edge, (b) ice concentration along the trajectory drops below 20 %, at which point we assume new ice formation, or (c) the 7-year maximum tracking period is reached. Sea ice motion estimates are based on three drift products: OSI SAF's OSI-405-c motion product (Lavergne, 2016), CERSAT's MERGED-motion product (Girard-Ardhuin & Ezraty, 2012), and NSIDC's Polar Pathfinder daily motion vectors (version 4.1, (Tschudi et al., 2020). The latter product is only used during the summer months (June - August) prior to 2012. Ice concentration along the trajectories is derived from CERSAT, based on 85GHz SSM/I brightness temperatures. This product utilizes the ARTIST Sea Ice (ASI) algorithm and is available on a 12.5 km $\times$ 12.5 km grid (Ezraty et al., 2007). Bathymetric information was obtained from the International Bathymetry Chart of the Arctic Ocean (IBCAO, Jakobsson et al. (2012)).

2.4. Statistics

We use the Mann-Kendall test(Mann, 1945; Kendall, 1975) to detect trends in the sea-ice concentration timeseries. It is designed to detect monotonic trends, without assumptions on the underlying statistical distribution. The outcome is "decreasing", "no trend" or "increasing", and we consider the trend as significant if it has a p-value equal or less to than 0.05. Furthermore linear regressions are used to estimate the magnitude of the trends, and Pearson correlation is used to estimate how much of the variability in the time series can be explained by the linear trend.

3. Results & Discussion: Sea-ice concentration

This section addresses the variability and trends of sea-ice concentration at the selected stations. To this end, we first look at time series of sea-ice concentration at each station. Subsequently, we investigate whether there are significant trends in mean sea-ice concentration over the N and EG clusters. Lastly, we extend our analysis by discussing anomalies in the larger surroundings of the HAUSGARTEN area. Here and in the following, we will refer to sea-ice concentration in absolute values, for example an increase from 10 % to 20 % will be referred to as an increase by 10 % (absolute increase), instead of an increase by 100 % (relative increase).

3.1. Annual trends

The time series in Figure 2 show that, generally, the sea-ice concentration decreases from east to west: While the average sea-ice concentration over the westernmost mooring is 77.4 %, it is only 7 % over the easternmost mooring (mooring locations are shown in Fig. 1). The statistical distribution of sea-ice concentration (Fig. 2h) is largely similar over the two westernmost moorings and then starts to decrease. The sea-ice concentration over moorings EG-II (Fig. 2b) and EG-III (Fig. 2) is identical because they share the same closest satellite pixel. We explain the meridional gradient of sea-ice concentration by the hydrographic conditions (Rudels and Carmack, 2022): The tongue of ice along the Greenland Coast is formed by ice which is exported out of Fram Strait, while at the same time the warm Atlantic water from the West Spitsbergen Current makes the eastern part of Fram Strait almost ice-free. Our results confirm that the sea-ice conditions in Fram Strait are driven by dynamics and not by the overall decline of Arctic-wide sea-ice extent. It is notable that the standard deviation of all monthly averages over 37 years (grey boxes in Fig. 2) is of similar magnitude for all moorings except N5 and N3. There are ice-free months over each mooring even for the westernmost mooring EG-I, although the period in which ice-free months can be observed only starts in 2000, while the first ice-free months over mooring EG-IV and the N cluster go back to 1990.

There is sub-monthly variability over each mooring which we smear out by only looking at monthly means. We quantify this by giving the monthly standard deviation for each station, i.e. the standard deviation of all days within each month (grey error bars in Fig. 2a)-g)). The median of these standard deviations is highest for the central moorings EG-IV and N5 (10.8 %),

between 5 and 10 % over EG-I, EG-II/III and N4 and lowest over N3 (3.8 %). In single months, it exceeds 30 % over each mooring.
Fig. 2i) shows that while the meridional gradient is fairly constant throughout the entire time, there can still be months every couple of years in which none of the moorings is covered by ice. In contrast, there is no month in which all stations were completely covered by sea ice. We ran a Mann-Kendall test for the time series at each station. No trend was detected for the N cluster and mooring EG-IV. A decreasing trend was detected over the moorings EG-I,II and III, but with slopes of only up to 1.2 %/decade.

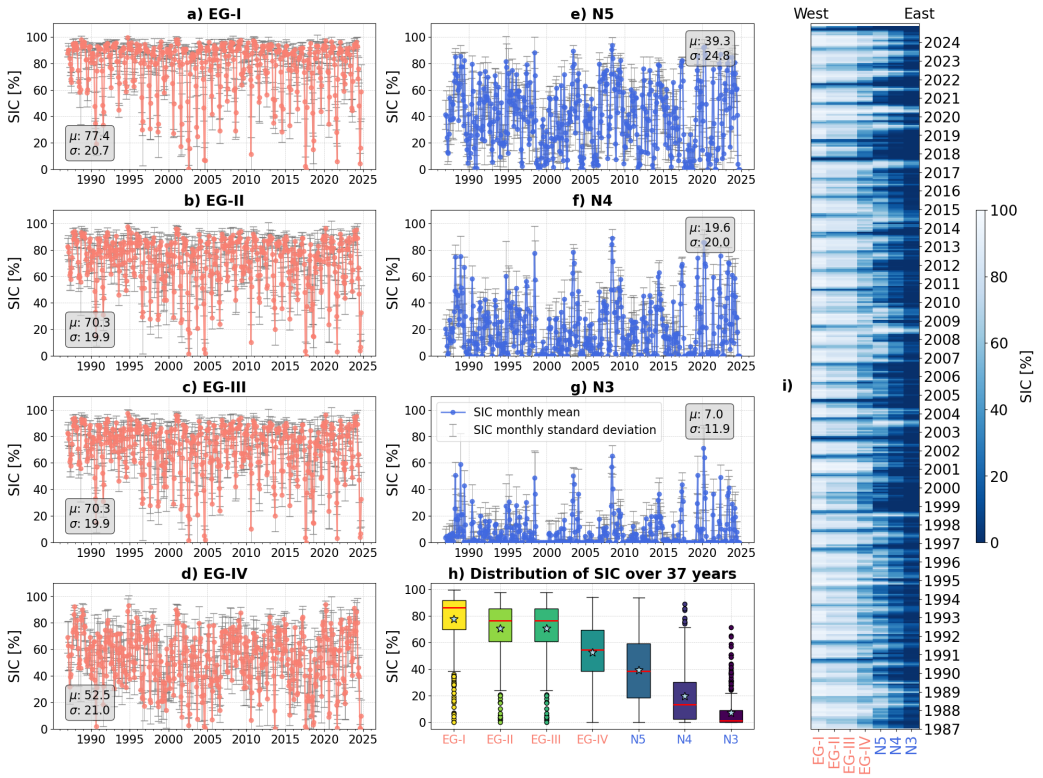

Figure 2: a) - g): Monthly mean sea-ice concentration at each mooring, with the mooring ID given in the caption. The x-axis shows the years, the y-axis shows the monthly mean sea-ice concentration at the respective mooring. The grey bars show the standard deviation between all days in the respective month. The grey boxes give the mean and standard deviation of the time series shown in the respective panel. h) Boxplots of the sea-ice concentration throughout the entire time period, with the black star showing the mean and the red line showing the median. They are color-coded to illustrate that they go from west (yellow) to east (dark blue), without a specific value being attached to the color. i) Heatmap showing the sea-ice concentration at each station for each year, sorted from West (left) to East (right).

3.2. Monthly trends

In this section, we extend the previous chapter's analysis by examining monthly time series. This is done separately for the EG and the N cluster, but not for each mooring. Instead, the values for each cluster are averaged. We show the resulting time series with linear fits in Fig. 3 (EG cluster) and Fig. 4 (N cluster).

Over the EG cluster, the sea-ice concentration has slopes of less than

2.0 %/decade for all months except August, September and October. August, September and October show larger and significant trends with up to -6.0 %/decade. The coefficient of determination (R^2 in Fig. 3 and Fig. 4) is 0.14 in October and smaller in the other months. This means that at most 14 % of the variability in the time series can be explained by the linear fit, even for the months with comparably large slopes. Furthermore, a Mann Kendall test yielded no significant trends for all months except August. This points to the fact that the increasing ice export described in Smedsrud et al. (2017); Zamani et al. (2019) and Krumpen et al. (2016) does not affect sea-ice concentration in Fram Strait. Also, warming events like the ones in April 2015 and April 2020 (Rostosky and Spreen, 2023) do not have a significant impact here.

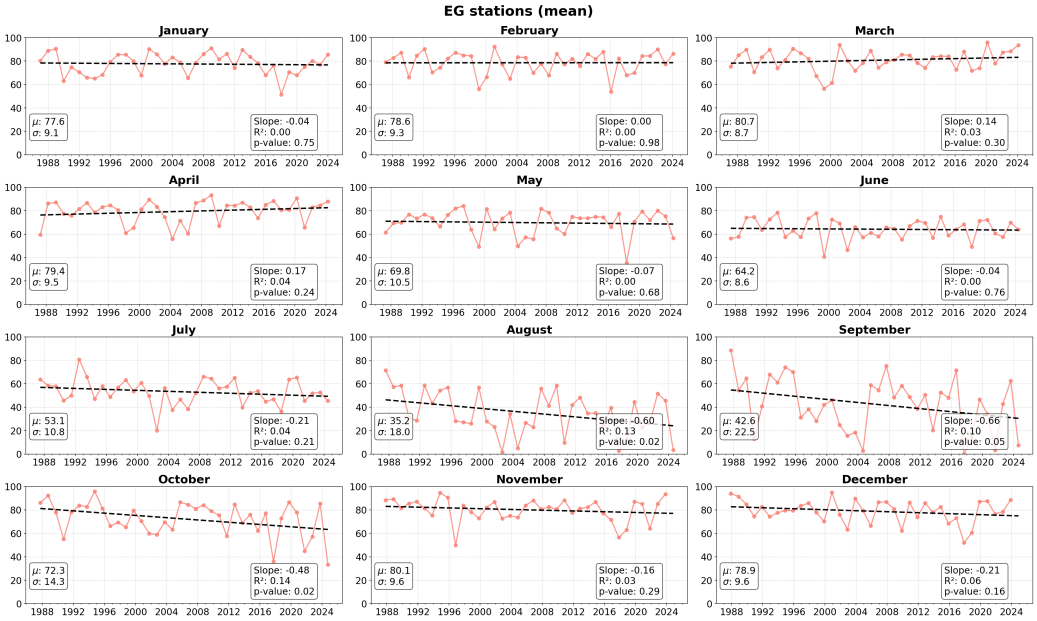

Figure 3: Monthly mean sea-ice concentration between 1987 and 2024, averaged over all stations in the EG cluster and separated by month, with the month given in the title of each panel. The dashed line shows the result of a linear regression, with the slope, the correlation coefficient and the p-value given in the text box on the lower left of each panel.

Over the N cluster, the average sea-ice concentration is below 40 % for each month. Interestingly, the sea-ice concentration is highest in April, May and June, when the Arctic-wide sea-ice extent is already declining. Slopes are generally higher over the N cluster than over the EG cluster. However,

the p-values are above 0.05 for all months except May. Here, the slope is 6.4 %/decade. The coefficient of determination in May is 0.11, so that 11 % of the variability in the time series can be explained by a linear trend.

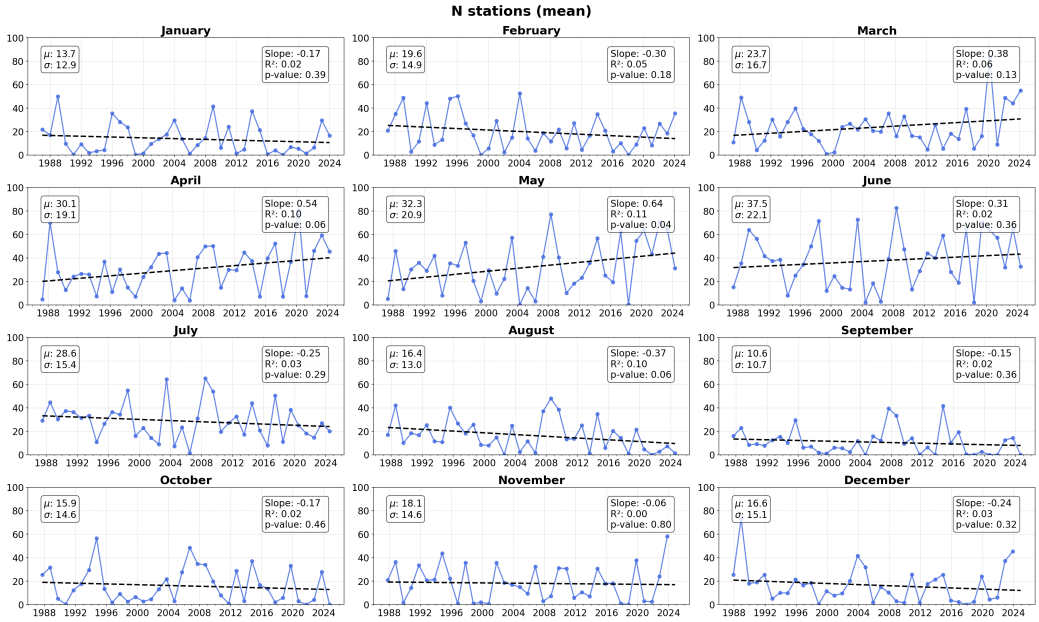

Figure 4: Monthly mean sea-ice concentration between 1987 and 2024, averaged over all stations in the N cluster and separated by month, with the month given in the title of each panel. The dashed line shows the result of a linear regression, with the slope, the correlation coefficient and the p-value given in the text box on the lower left of each panel.

3.3. Sea-ice concentration in the surroundings

We continue our analysis by investigating sea-ice concentration and its anomalies in the region around HAUSGARTEN. Monthly-mean maps of the July sea-ice concentration are shown in Fig. 5. We focus on the period since 2015 since earlier years have already been briefly covered in Soltwedel et al. (2016). The Northeast Water Polynya (Bennett et al., 2024) was open in each year since 2015 and partly extended towards the western part of the EG cluster (e.g. in 2017). The highly variable sea-ice conditions from the time series at the moorings are manifestations of the larger-scale patterns: While the region north of 82°N is completely ice-covered each year, the sea-ice concentration in Barents Sea and Fram Strait are more variable. Barents Sea is mostly ice-free, but was partly ice-covered in 2017 and 2019. The ice conditions in Fram Strait vary more strongly than in the Barents Sea. Both clusters are mostly located at the highly dynamical sea-ice marginal zone. The EG cluster is located within the ice pack (red contour line in Fig. 5) in each year. It is, however, always close to the open ocean. The part between the EG cluster and the Greenland coastline is ice-covered in most years, but the sea-ice concentration is still below 100 %, indicating a loose ice cover which is prone to the influence of dynamics. The N cluster is located on the 15 % contour line in all years and thus captures the transition from the ice pack to the open water. The westernmost mooring N5 is always inwards or at the 15 % contour line, while the easternmost mooring N3 is in most years outside of the 15 % contour line. In some years (2015, 2017, 2020), the eastern coast of Svalbard is covered by sea ice, while it is ice-free in the other years.

To investigate how the sea-ice conditions changed since 2015, we show sea-ice concentration anomalies in Fig. 6. For anomalies in earlier years, we refer the reader to Soltwedel et al. (2016). Our reference period (1981–2000) was chosen to be consistent with Soltwedel et al. (2016). The anomalies over the region north of 82°N are positive in most years until 2019, but slightly negative afterwards. Large negative anomalies are evident over the Barents Sea, meaning that the sea-ice cover declined by more than 50 % compared to the reference period. This does not affect Fram Strait, where there is no clear pattern over the EG and N clusters and the sea-ice conditions are rather dominated by year-to-year variability.

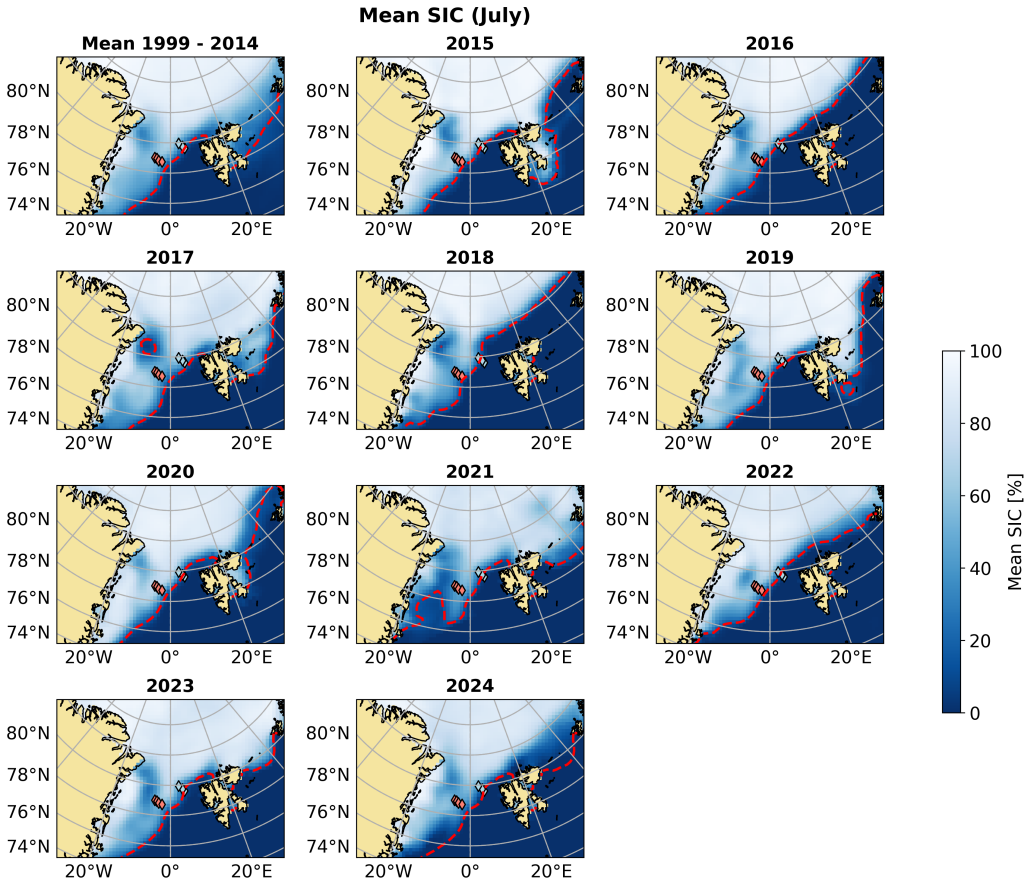

Figure 5: a) Average July sea-ice concentration between 1999 and 2014 (see Soltwedel et al. (2016) for earlier dates before that period). b) - k) Average July sea-ice concentration in 2015-2024, with the respective year given in the title of each panel. Values are given in percent.

4. Results & Discussion: Origin and Age

Using satellite-derived sea ice motion products, we backtracked the ice passing the EGI-IV (western) and N3-5 (eastern) mooring locations in Fram Strait to their areas of origin (see Methods: "Backtrajectories of sea ice" for details). The trajectories starting from a position in the centre of N3-5 and EGI-IV are shown in Figure 7. It is apparent that ice observed at both locations predominantly originates from the Russian shelf seas (see also Swoboda et al. (2024)). The western location (EGI-IV), however, can also receive ice

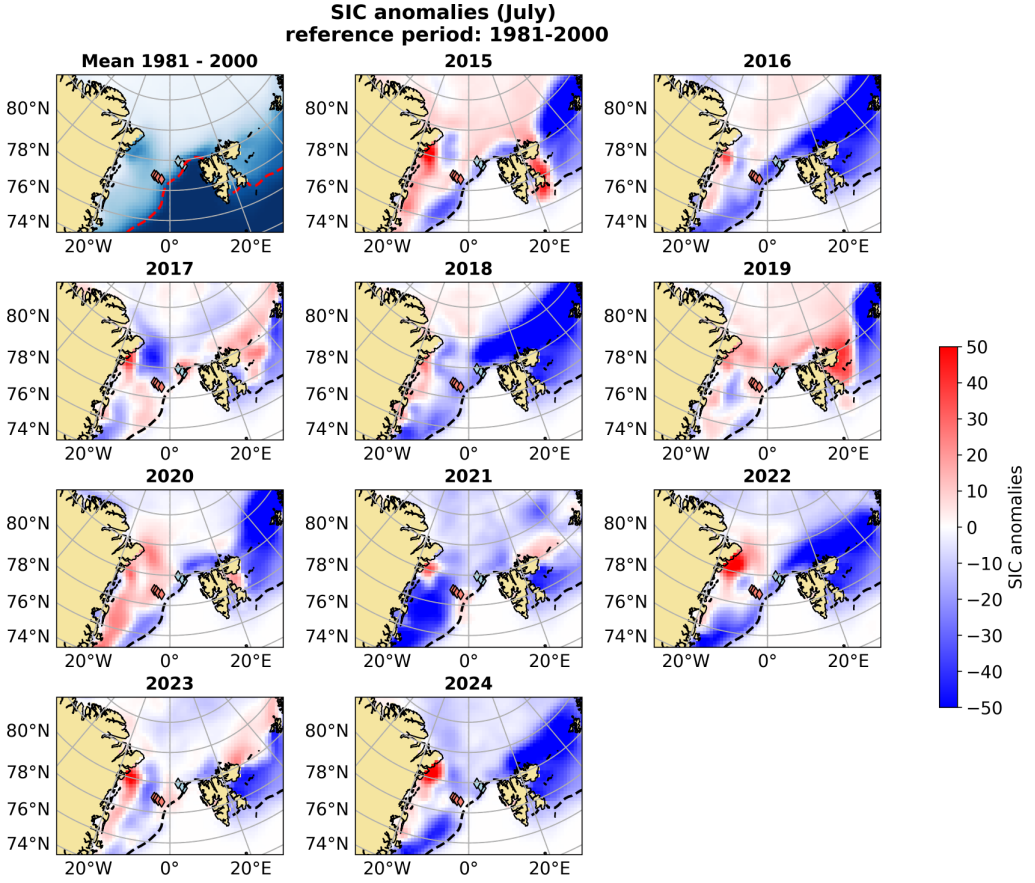

Figure 6: a) Mean sea-ice concentration in July, averaged between 1981 and 2000. b) – k) Difference between July sea-ice concentration in the respective year and the average July sea-ice concentration from 1981-2000 (panel a). The respective year is given in the panel's title, the colorbar ranges from -50 to 50 %.

sourced from the Beaufort Gyre. Because the western site remains consistently ice-covered (Fig. 3), we have been able to compute backtrajectories almost every month. In contrast, the eastern moorings (N3-5) experienced more intermittent ice coverage, resulting in fewer trajectories and limiting robust trend analyses at that location.

4.1. Changing ice age

Examining changes in sea-ice age at both sites over the past three decades reveals a pronounced and statistically significant decline (Fig. 8, EGI-IV: -

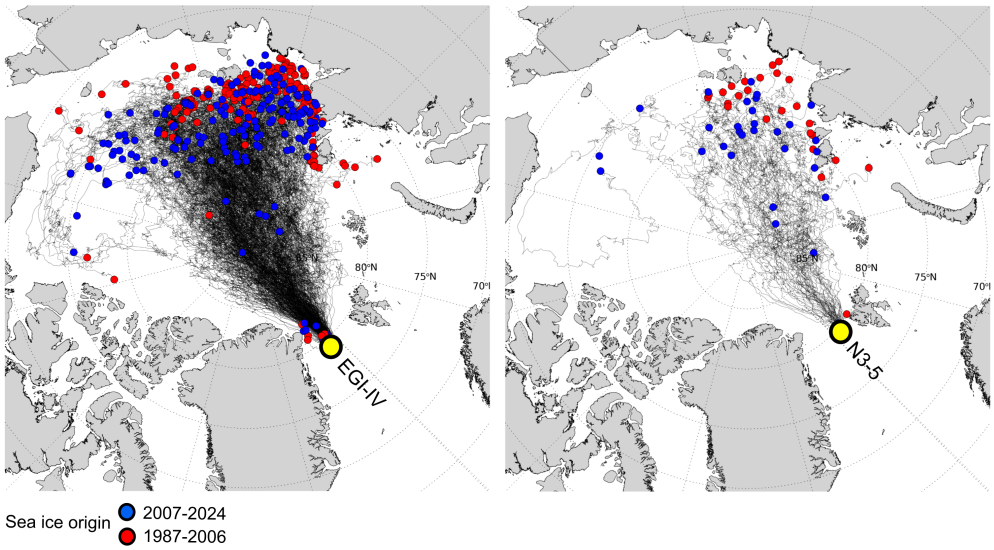

Figure 7: Backtrajectories of sea ice passing by the EGI-IV (left) and N3-5 (right) mooring locations. Trajectories (black lines) were calculated monthly from January, 1987, to September, 2024. Sea ice origins are marked by red dots for ice formed before 2006 and blue dots for ice formed after 2007, illustrating shifts in ice origin over time.

281 d/decade, N3-5: -258 d/decade). The stepwise decrease in multiyear ice age, previously noted in the central Arctic Ocean (Babb et al., 2023), is also evident in the western Fram Strait. In the late 1980s, the ice passing over the moorings was, on average, 4 years old. This was followed by an era in the 1990s to mid-2000s dominated by 3-year-old ice, and since 2005, by predominantly 2-year-old ice. The reductions are associated with episodic export of old ice through Fram Strait, faster ice drift and reduced residence time ((Sumata et al., 2023), as well as changes in atmospheric circulation and enhanced melting due to warming atmosphere and oceans ((Babb et al., 2023), (Maslanik et al., 2011)). In line with Sumata et al. (2023), this ongoing reduction in ice age has occurred alongside decreasing ice thickness and reduced frequency of pressure ridges (Krumpen et al., 2025).

4.2. Shifting ice origin

In addition to the reduced transit time of sea ice, we find that the origin of ice passing both sites has shifted northward over time. Figure 9 shows the annual fraction of ice originating from shallow shelf areas (defined as

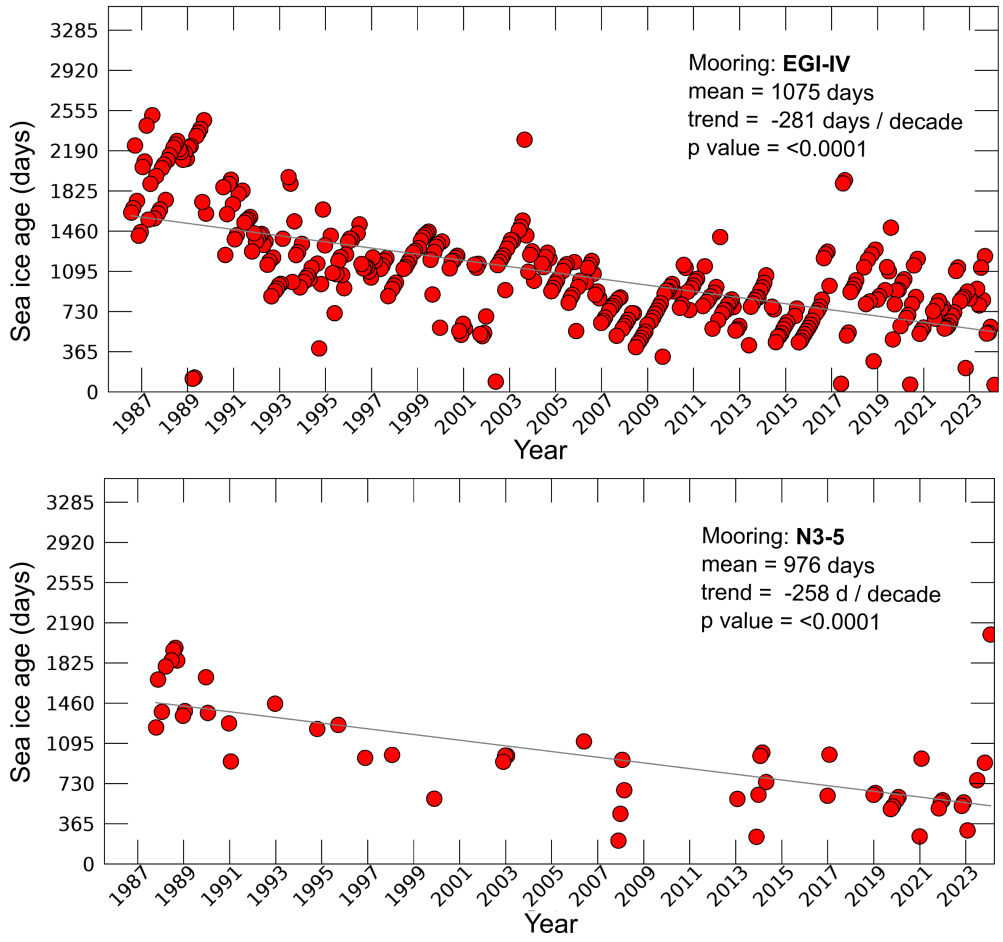

Figure 8: Sea ice age (in days) passing by the EGI-IV (top) and N3-5 (bottom) mooring locations. Ice age was determined based on the length of the backtrajectories shown in Fig. 7. Trend lines and statistical metrics are included in each graph.

regions with water depths <50 m). Ice formed in these shallow zones often develops during polynya events and can incorporate suspended sediments and other biogeochemical constituents during its formation. The statistically significant decline in the fraction of ice originating from shallow waters (EGI-IV: -11.5 %/decade) is the consequence of a reduced survival rates of newly formed ice in a warming Arctic (Krumpen et al., 2019). Although the ice produced over shallow shelves continues to be advected northward, it now more frequently melts during the following summer, thus interrupting

the transport of sediments and organic material towards Fram Strait. This effect is also evident at sediment traps deployed at HAUSGARTEN sites: Following Swoboda et al. (2024), the terrigenous fluxes from melting sea ice in Fram Strait decreased by more than 80 % between 2000 and 2013. The northward shift in ice origin from shallow to deeper sites is also visible in Figure 7. Red points represent sea ice origins of trajectories from the earlier period (1987–2006), while blue points indicate formation sites of more recent trajectories (2007–2024).

The accuracy of the backtrajectories depends on the quality of the underlying sea ice motion products. Sumata et al. (2014) compared various motion datasets and showed that accuracy can be limited, especially during summer due to surface melt, and that substantial differences exist among products. To assess tracking quality, Krumpen et al. (2019) reproduced the trajectories of GPS buoys using IceTrack. After 200 days, the discrepancy between actual and virtual buoy positions averaged 36 ± 20 km, which is sufficiently small to instill confidence in our ice age and origin estimates. However, errors are generally larger during the initial tracking phase, as long as the ice is located in Fram Strait. According to Krumpen et al. (2020), this is due to the challenging and dynamic ice conditions that are characteristic for the narrow region between Greenland and Svalbard, which complicate accurate sea ice motion retrieval.

5. Conclusions

We analysed how sea-ice concentration, origin and age in the HAUSGARTEN area changed since 1987. The research questions which were raised at the end of section 1 can now be answered as follows:

1. **How does the sea-ice concentration over the HAUSGARTEN moorings change between 1987 and 2024?**

There is no noticeable long-term trend at any of the moorings, neither in the overall magnitude nor in the variability of sea ice. When analyzing trends by month, we observe weak but statistically significant decreases from August to September at the EGI-IV (western) moorings, and a weak but significant increase in May at the N3-5 (eastern) moorings. We attribute the general lack of pronounced trends to the continuous inflow of sea ice from the north into the HAUSGARTEN region, which diminishes the impact of processes

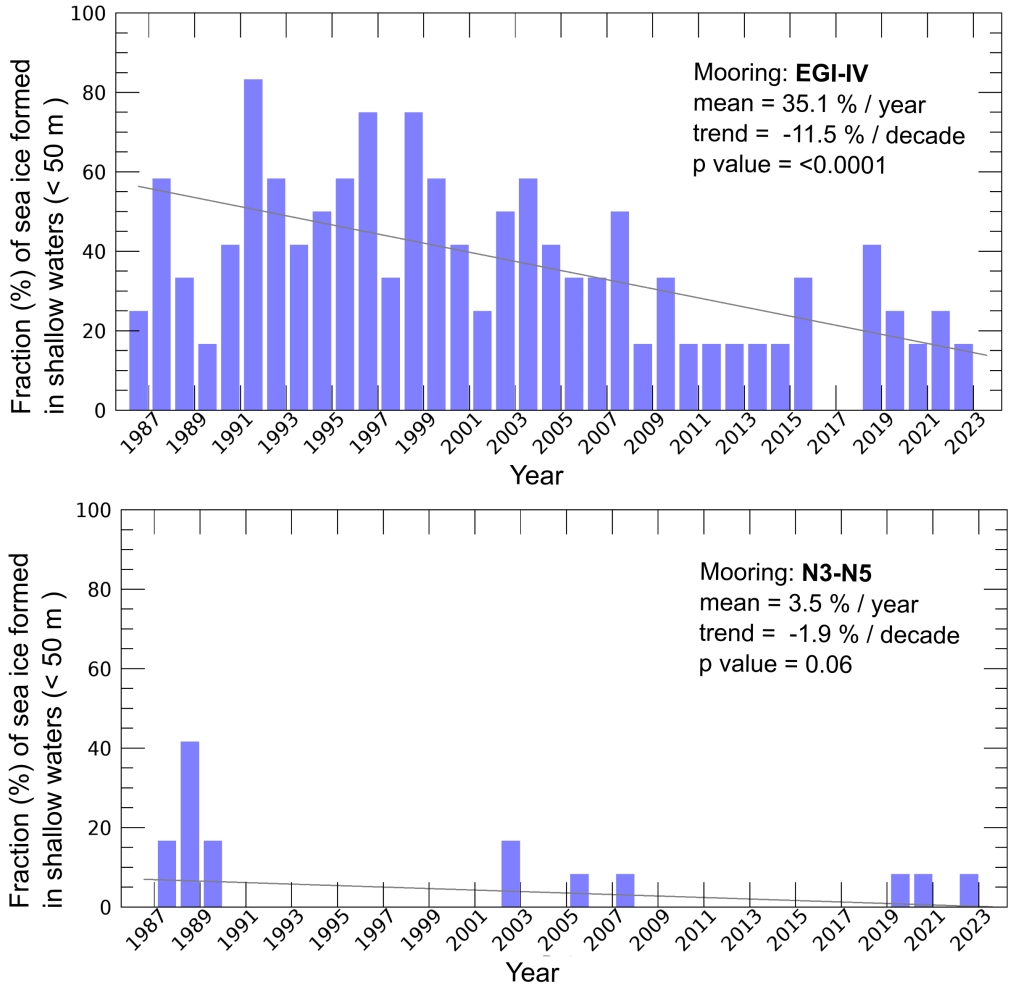

Figure 9: Annual fraction (%) of sea ice originating from shallow shelf regions (<50 m depth) at the EGI-IV and N3-5 mooring sites January, 1987 and September, 2024. Trend lines and statistical metrics are included in each graph

favoring sea-ice melt.

2. **How do sea-ice properties (origin and age) of sea ice drifting over the HAUSGARTEN moorings change during this period?**

Sea ice passing over both the EGI-IV (western) and N3–5 (eastern) moorings predominantly originates from the Russian shelf seas, with occasional contributions from the Beaufort Gyre at the western site. Over the past three decades, its average age has declined significantly—from about four years in the late 1980s to around two years since 2005—and its origin has shifted northward. As a result, the fraction of sea ice at the HAUSGARTEN sites originating from shallow-shelf regions is decreasing, and so is the amount of ice-rafted matter that becomes entrained during ice formation.

6. Acknowledgments

VL acknowledges funding from the ESA project Sea-Ice Thickness Intercomparison Exercise (SIN'XS).

References

von Appen, W.J., Waite, A.M., Bergmann, M., Bienhold, C., Boebel, O., Bracher, A., Cisewski, B., Hagemann, J., Hoppema, M., Iversen, M.H., et al., 2021. Sea-ice derived meltwater stratification slows the biological carbon pump: results from continuous observations. Nature Communications 12, 7309.

Babb, D.G., Galley, R.J., Kirillov, S., Landy, J.C., Howell, S.E.L., Stroeve, J.C., Meier, W., Ehn, J.K., Barber, D.G., 2023. The stepwise reduction of multiyear sea ice area in the arctic ocean since 1980. Journal of Geophysical Research: Oceans 128, e2023JC020157. URL: https://agupubs.onlinelibrary.wiley.com/doi/abs/10.1029/2023JC020157, doi:https://doi.org/10.1029/2023JC020157, arXiv:https://agupubs.onlinelibrary.wiley.com/doi/pdf/10.1029/2023JC020157. e2023JC020157 2023JC020157.

Belter, H.J., Krumpen, T., von Albedyll, L., Alekseeva, T.A., Birnbaum, G., Frolov, S.V., Hendricks, S., Herber, A., Polyakov, I., Raphael, I., Ricker, R., Serovetnikov, S.S., Webster, M., Haas, C., 2021. Interannual variability in transpolar drift summer sea ice thickness and potential impact of atlantification. The Cryosphere 15, 2575–2591. URL: https://tc.copernicus.org/articles/15/2575/2021/, doi:10.5194/tc-15-2575-2021.

Bennett, M.G., Renfrew, I.A., Stevens, D.P., Moore, G.W.K., 2024. The northeast water polynya, greenland: Climatology, atmospheric forcing and ocean response. Journal of Geophysical Research: Oceans 129, e2023JC020513. URL: https://agupubs.onlinelibrary.wiley.com/doi/abs/10.1029/2023JC020513, doi:https://doi.org/10.1029/2023JC020513, arXiv:https://agupubs.onlinelibrary.wiley.com/doi/pdf/10.1029/2023JC020513. e2023JC020513 2023JC020513.

Bergmann, M., Allen, S., Krumpen, T., Allen, D., 2023. High levels of microplastics in the arctic sea ice alga melosira arctica, a vector to ice-associated and benthic food webs. Environmental Science & Technology 57, 6799–6807. URL: https://doi.org/10.1021/acs.est.2c08010, doi:10.1021/acs.est.2c08010, arXiv:https://doi.org/10.1021/acs.est.2c08010. pMID: 37083047.

Bergmann, M., Wirzberger, V., Krumpen, T., Lorenz, C., Primpke, S., Tekman, M.B., Gerdts, G., 2017. High quantities of microplastic in arctic deep-sea sediments from the hausgarten observatory. Environmental Science & Technology 51, 11000–11010. URL: https://doi.org/10.1021/acs.est.7b03331, doi:10.1021/acs.est.7b03331, arXiv:https://doi.org/10.1021/acs.est.7b03331. pMID: 28816440.

Botterell, Z.L., Bergmann, M., Hildebrandt, N., Krumpen, T., Steinke, M., Thompson, R.C., Lindeque, P.K., 2022. Microplastic ingestion in zooplankton from the fram strait in the arctic. Science of The Total Environment 831, 154886. URL: https://www.sciencedirect.com/science/article/pii/S0048969722019799, doi:https://doi.org/10.1016/j.scitotenv.2022.154886.

Brodzik, M.J., Billingsley, B., Haran, T., Raup, B., Savoie, M.H., 2012. Easegrid 2.0: Incremental but significant improvements for earth-gridded data sets. ISPRS International Journal of Geo-Information 1, 32–45. URL: https://www.mdpi.com/2220-9964/1/1/32, doi:10.3390/ijgi1010032.

Cardozo-Mino, M.G., Salter, I., Nöthig, E.M., Metfies, K., Ramondenc, S., Wekerle, C., Krumpen, T., Boetius, A., Bienhold, C., 2023. A decade of microbial community dynamics on sinking particles during high carbon export events in the eastern fram strait. Frontiers in Marine Science 10. URL: https://www.frontiersin.org/journals/marine-science/articles/10.3389/fmars.2023.1173384, doi:10.3389/fmars.2023.1173384.

Ezraty, R., Girard-Ardhuin, F., Piolle, J.F., Kaleschke, L., Heygster, G., 2007. Arctic and Antarctic Sea Ice Concentration and Arctic Sea Ice Drift Estimated from Special Sensor Microwave Data. Technical Report. IFREMER.

Jakobsson, M., Mayer, L., Coakley, B., Dowdeswell, J.A., Forbes, S., Fridman, B., Hodnesdal, H., Noormets, R., Pedersen, R., Rebesco, M., Schenke, H.W., Zarayskaya, Y., Accettella, D., Armstrong, A., Anderson, R.M., Bienhoff, P., Camerlenghi, A., Church, I., Edwards, M., Gardner, J.V., Hall, J.K., Hell, B., Hestvik, O., Kristoffersen, Y., Marcussen, C., Mohammad, R., Mosher, D., Nghiem, S.V., Pedrosa, M.T., Travaglini, P.G., Weatherall, P., 2012. The international bathymetric chart of the arctic ocean (ibcao) version 3.0. Geophysical Research Letters

39. URL: https://agupubs.onlinelibrary.wiley.com/doi/abs/10.1029/2012GL052219, doi:https://doi.org/10.1029/2012GL052219, arXiv:https://agupubs.onlinelibrary.wiley.com/doi/pdf/10.1029/2012GL052219.

Kendall, M.G., 1975. Rank correlation methods. 4 ed., Charles Griffin.

Krumpen, T., von Albedyll, L., Bünger, H.J., Castellani, G., Hartmann, J., Helm, V., Hendricks, S., Hutter, N., Landy, J., Lisovski, S., Lüpkes, C., Rohde, J., Suhrhoff, M., Haas, C., 2025. Smoother ice in a more dynamic arctic: 30 years of airborne pressure ridge observations. Nature Climate Change URL: https://oceanrep.geomar.de/id/eprint/61034/. in Press / Accepted.

Krumpen, T., Belter, H.J., Boetius, A., Damm, E., Haas, C., Hendricks, S., Nicolaus, M., Nöthig, E.M., Paul, S., Peeken, I., et al., 2019. Arctic warming interrupts the Transpolar Drift and affects long-range transport of sea ice and ice-rafted matter. Scientific reports 9, 5459.

Krumpen, T., Birrien, F., Kauker, F., Rackow, T., von Albedyll, L., Angelopoulos, M., Belter, H.J., Bessonov, V., Damm, E., Dethloff, K., Haapala, J., Haas, C., Harris, C., Hendricks, S., Hoelemann, J., Hoppmann, M., Kaleschke, L., Karcher, M., Kolabutin, N., Lei, R., Lenz, J., Morgenstern, A., Nicolaus, M., Nixdorf, U., Petrovsky, T., Rabe, B., Rabenstein, L., Rex, M., Ricker, R., Rohde, J., Shimanchuk, E., Singha, S., Smolyanitsky, V., Sokolov, V., Stanton, T., Timofeeva, A., Tsamados, M., Watkins, D., 2020. The mosaic ice floe: sediment-laden survivor from the siberian shelf. The Cryosphere 14, 2173–2187. URL: https://tc.copernicus.org/articles/14/2173/2020/, doi:10.5194/tc-14-2173-2020.

Krumpen, T., Gerdes, R., Haas, C., Hendricks, S., Herber, A., Selyuzhenok, V., Smedsrud, L., Spreen, G., 2016. Recent summer sea ice thickness surveys in fram strait and associated ice volume fluxes. The Cryosphere 10, 523–534. URL: https://tc.copernicus.org/articles/10/523/2016/, doi:10.5194/tc-10-523-2016.

Kwok, R., Spreen, G., Pang, S., 2013. Arctic sea ice circulation and drift speed: Decadal trends and ocean currents. Journal of Geophysical Research: Oceans 118, 2408–2425. URL: https://agupubs.onlinelibrary.wiley.com/doi/abs/10.

1002/jgrc.20191, doi:https://doi.org/10.1002/jgrc.20191, arXiv:https://agupubs.onlinelibrary.wiley.com/doi/pdf/10.1002/jgrc.20191.

Lavergne, T., 2016. Validation and Monitoring of the OSI SAF Low-Resolution Sea Ice Drift Product. Technical Report. The EUMETSAT Network of Satellite Application Facilities.

Lavergne, T., Soerensen, A., Tonboe, R., Saldo, R., Pedersen, L.T., Strong, C., Cherkaev, E., Golden, K., Eastwood, S., 2022. Global Sea Ice Concentration Climate DataRecordsAlgorithm Theoretical Basis Document. Technical Report. OSI SAF/EUMETSAT.

Mann, H.B., 1945. Nonparametric tests against trend. Econometrica: Journal of the econometric society , 245–259.

Maslanik, J., Stroeve, J., Fowler, C., Emery, W., 2011. Distribution and trends in arctic sea ice age through spring 2011. Geophysical Research Letters 38. URL: https://agupubs.onlinelibrary.wiley.com/doi/abs/10.1029/2011GL047735, doi:https://doi.org/10.1029/2011GL047735, arXiv:https://agupubs.onlinelibrary.wiley.com/doi/pdf/10.1029/2011GL047735.

Roscher, L., Nöthig, E.M., Fahl, K., Wekerle, C., Krumpen, T., Hoppmann, M., Knüppel, N., Primpke, S., Gerdts, G., Bergmann, M., 2025. Origin and intra-annual variability of vertical microplastic fluxes in fram strait, arctic ocean. Science of The Total Environment 958, 178035. URL: https://www.sciencedirect.com/science/article/pii/S0048969724081920, doi:https://doi.org/10.1016/j.scitotenv.2024.178035.

Rostosky, P., Spreen, G., 2023. Relevance of warm air intrusions for arctic satellite sea ice concentration time series. The Cryosphere 17, 3867–3881. URL: https://tc.copernicus.org/articles/17/3867/2023/, doi:10.5194/tc-17-3867-2023.

Rudels, B., Carmack, E., 2022. Arctic ocean water mass structure and circulation. Oceanography 35, :52–65. URL: https://doi.org/10.5670/oceanog.2022.116.

Smedsrud, L.H., Halvorsen, M.H., Stroeve, J.C., Zhang, R., Kloster, K., 2017. Fram strait sea ice export variability and september arctic

sea ice extent over the last 80 years. The Cryosphere 11, 65–79. URL: https://tc.copernicus.org/articles/11/65/2017/, doi:10.5194/tc-11-65-2017.

Smedsrud, L.H., Sirevaag, A., Kloster, K., Sorteberg, A., Sandven, S., 2011. Recent wind driven high sea ice area export in the fram strait contributes to arctic sea ice decline. The Cryosphere 5, 821–829. URL: https://tc.copernicus.org/articles/5/821/2011/, doi:10.5194/tc-5-821-2011.

Soltwedel, T., Bauerfeind, E., Bergmann, M., Bracher, A., Budaeva, N., Busch, K., Cherkasheva, A., Fahl, K., Grzelak, K., Hasemann, C., Jacob, M., Kraft, A., Lalande, C., Metfies, K., Nöthig, E.M., Meyer, K., Quéric, N.V., Schewe, I., Włodarska-Kowalczuk, M., Klages, M., 2016. Natural variability or anthropogenically-induced variation? insights from 15 years of multidisciplinary observations at the arctic marine lter site hausgarten. Ecological Indicators 65, 89–102. URL: https://www.sciencedirect.com/science/article/pii/S1470160X15005361, doi:https://doi.org/10.1016/j.ecolind.2015.10.001.

Soltwedel, T., Bauerfeind, E., Bergmann, M., Budaeva, N., Hoste, E., Jaeckisch, N., von Juterzenka, K., Matthiessen, J., Mokievsky, V., Nöthig, E.M., Quéric, N.V., Sablotny, B., Sauter, E., Schewe, I., Urban-Malinga, B., Wegner, J., Wlodarska-Kowalczuk, M., Klages, M., 2005. Hausgarten: Multidisciplinary investigations at a deep-sea, long-term observatory in the arctic ocean. Oceanography 18, 46–61. URL: https://doi.org/10.5670/oceanog.2005.24.

Sumata, H., Lavergne, T., Girard-Ardhuin, F., Kimura, N., Tschudi, M.A., Kauker, F., Karcher, M., Gerdes, R., 2014. An intercomparison of arctic ice drift products to deduce uncertainty estimates. Journal of Geophysical Research: Oceans 119, 4887–4921. URL: https://agupubs.onlinelibrary.wiley.com/doi/abs/10.1002/2013JC009724, doi:https://doi.org/10.1002/2013JC009724, arXiv:https://agupubs.onlinelibrary.wiley.com/doi/pdf/10.1002/2013JC009724.

Sumata, H., de Steur, L., Divine, D.V., Granskog, M.A., Gerland, S., 2023. Regime shift in arctic ocean sea ice thickness. Nature 615, 443–449.

Swoboda, S., Krumpen, T., Nöthig, E.M., Metfies, K., Ramondenc, S., Wollenburg, J., Fahl, K., Peeken, I., Iversen, M., 2024. Re-

lease of ballast material during sea-ice melt enhances carbon export in the arctic ocean. PNAS Nexus 3, pgae081. URL: https://doi.org/10.1093/pnasnexus/pgae081, doi:10.1093/pnasnexus/pgae081, arXiv:https://academic.oup.com/pnasnexus/article-pdf/3/4/pgae081/57336229/pgae081.pdf.

Taylor, J., Krumpen, T., Soltwedel, T., Gutt, J., Bergmann, M., 2016. Regional- and local-scale variations in benthic megafaunal composition at the arctic deep-sea observatory hausgarten. Deep Sea Research Part I: Oceanographic Research Papers 108, 58–72. URL: https://www.sciencedirect.com/science/article/pii/S096706371530042X, doi:https://doi.org/10.1016/j.dsr.2015.12.009.

Taylor, J., Krumpen, T., Soltwedel, T., Gutt, J., Bergmann, M., 2017. Dynamic benthic megafaunal communities: Assessing temporal variations in structure, composition and diversity at the arctic deep-sea observatory hausgarten between 2004 and 2015. Deep Sea Research Part I: Oceanographic Research Papers 122, 81–94. URL: https://www.sciencedirect.com/science/article/pii/S0967063716302485, doi:https://doi.org/10.1016/j.dsr.2017.02.008.

Tekman, M.B., Krumpen, T., Bergmann, M., 2017. Marine litter on deep arctic seafloor continues to increase and spreads to the north at the hausgarten observatory. Deep Sea Research Part I: Oceanographic Research Papers 120, 88–99. URL: https://www.sciencedirect.com/science/article/pii/S096706371630200X, doi:https://doi.org/10.1016/j.dsr.2016.12.011.

Tschudi, M.A., Meier, W.N., Stewart, J.S., 2020. An enhancement to sea ice motion and age products at the national snow and ice data center (nsidc). The Cryosphere 14, 1519–1536. URL: https://tc.copernicus.org/articles/14/1519/2020/, doi:10.5194/tc-14-1519-2020.

Wekerle, C., Krumpen, T., Dinter, T., von Appen, W.J., Iversen, M.H., Salter, I., 2018. Properties of sediment trap catchment areas in fram strait: Results from lagrangian modeling and remote sensing. Frontiers in Marine Science 5. URL: https://www.frontiersin.org/journals/marine-science/articles/10.3389/fmars.2018.00407, doi:10.3389/fmars.2018.00407.

Zamani, B., Krumpen, T., Smedsrud, L.H., Gerdes, R., 2019. Fram strait sea ice export affected by thinning: comparing high-resolution simulations and observations. Climate Dynamics 53, 3257–3270.